Journal of Power Sources 248 (2014) 457–464

Contents lists available at ScienceDirect

Journal of Power Sources

journal homepage: www.elsevier.com/locate/jpowsour

In situ Scanning electron microscope study and microstructural evolution of nano silicon anode for high energy Li-ion batteries

P. Hovington [a], M. Dontigny [a], A. Guerfi [a], J. Trottier [a], M. Lagacé [a], A. Mauger [b], C.M. Julien [c], K. Zaghib [a,*]

[a] Energy Storage and Conversion, Institut de Recherche Hydro-Québec, Varennes, QC, Canada J3X 1S1
[b] Université Paris 6, IMPMC, 4 Place Jussieu 75252 Paris Cedex 05, France
[c] Université Paris 6, PECSA, 4 Place Jussieu 75005 Paris, France

HIGHLIGHTS

- Volumic expansion of nano Si was observer by in situ SEM.
- Si keep their integrity when the discharge is stopped at a voltage 0.1 V.
- Particles of size $d < 2$ μm do not crack.

GRAPHICAL ABSTRACT

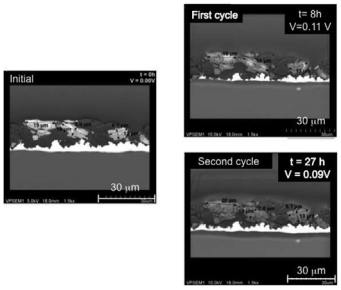

ARTICLE INFO

Article history:
Received 16 July 2013
Received in revised form
13 September 2013
Accepted 16 September 2013
Available online 5 October 2013

Keywords:
Nano Si
In situ SEM
Anode
Li-ion
High energy battery

ABSTRACT

In situ and ex situ scanning electron microscopy of nano Si and SiO anode particles was carried out during the first cycles, and at various stages of charge. The particle size effects were explored in the range 0.1–20 μm, providing a new insight into the micro-structural evolution of the particles as a function of their size, and into the 'mechanical' resistance upon important volume change upon phase transformation of these anodes. For small particles, the failure of the battery comes from an electrochemical sintering that compacts the whole electrode, which results in its cracking. The particles keep their integrity when the discharge is stopped at a voltage 0.1 V, which corresponds to the chemical composition $Li_{12}Si_7$, while the particles are known to crack at deeper discharge up to $Li_{22}Si_5$. Replacing the Si particles by SiO particles in an attempt to avoid these structural effects did not help, because of the different chemical reactions during cycling, with the loss of oxygen.

1. Introduction

Lithium-ion batteries have become the most popular technology for electric energy storage, with applications as power source for portable electronics, and more recently for hybrid and electric vehicles. This success is due to the development and optimization of active materials as positive electrodes (see Refs. [1–3] for a review), and negative electrodes (see Ref. [4] for a review). Many efforts are currently made to increase the energy density, the power density and the intrinsic safety of the battery. The commercialized anode is usually graphite carbon, although $Li_4Ti_5O_{12}$ is presently used for applications that demand a lot of power [5,6]. The capacity of carbon graphite is 370 mAh g^{-1}. This is much smaller than silicon that has a gravimetric capacity 4200 mAh g^{-1} when lithiated to

* Corresponding author.
E-mail address: zaghib.karim@ireq.ca (K. Zaghib).

0378-7753/$ – see front matter © 2013 Elsevier B.V. All rights reserved.
http://dx.doi.org/10.1016/j.jpowsour.2013.09.069

$Li_{4.4}Si$, and volumetric density 9786 mAh cm^{-3} based on the initial volume of Si, respectively [7–9]. These are the highest capacities among all the anode elements for Li-ion batteries, except Li metal itself. For this reason, Si has been considered as the promising element to increase the energy density of the Li-ion batteries since many years [10–12]. It is, however, difficult to believe it, because the cathode limits the energy density of a Li-ion cell, not by the anode element. The capacity of $LiFePO_4$ olivine is 170 mAh g^{-1}, that of lamellar compounds slightly larger, but still much smaller than that of graphite, and at the price of thermal instability that reduces the intrinsic safety of the batteries [13]. Nevertheless, the investigation on the Si anode is of interest for another reason, as the performance of the graphite anode depends strongly on the stabilization and control of the solid–electrolyte interface that limits the performance and calendar life of the battery. So far however, Si-based anodes suffer from numerous problems that prevent them being commercialized. In particular, the performance degrades during the first cycles due to the large variations of the volume during the charging/discharging process [14–20]: when transforming from Si to $Li_{4.4}Si$, the volume expansion is 420% [21–25]. This large volume expansion/contraction during lithium insertion/extraction is responsible for the cracking of the Si particles, observed by atomic force microscopy during the Li-extraction [26–28]. In an attempt to overcome this problem, many efforts have been made to reduce the size of the Si particles to the nanoscale, which have been recently reviewed [29], in order to reduce the internal stress, Indeed, the electrochemical properties have been improved when Si is under the from of clamped hollow structures, such as double-walled nanotubes and yolk-shell nanoparticles. Such a structure, with Si nanotubes coated with a SiO_x layer showed a remarkable capacity of 1000 mAh g^{-1} at rate 12C, with long cycling life (6000 cycles with 88% capacity retention) [30]. Such devices, however, are still too expensive to be commercialized. In this context, the size dependence of the Si-properties and the nature of the solid–electrolyte interface need to be studied and are identified as two areas where research is needed [29]. For this purpose, in-situ electron microscopy measurements are a very useful tool, since they allow real-time observation of the charging/discharging behavior of individual particles. This strategy has already been used to investigate the effect of metallic coating on Si expansion [20], and the behavior of individual Si nanowire electrodes [31–34].

In the present work, we report both in-situ and ex-situ SEM experiments to observe the charging/discharging behavior of bigger particles to investigate the micro-structural evolution of nano Si particles during electrochemical cycling as a function of their size, completed by an analysis of SiO-based anode, aiming to determine the critical size above which cracking of bare particles cannot be avoided. We also investigate dynamically the micro-structural change of morphology of the whole Si and SiO electrodes to investigate the effect of the changes of the volumes of the particles at the level of the entire electrode (active material, binder, conductive carbon).

2. Experimental

2.1. Materials

Different sources of Si were selected to cover a broader range of particle sizes: nano-Si particles (average particle size ca. 100 nm); bigger SiO_x particles (2–8 μ). 0.8 cm × 0.8 cm cells were assembled and prepared for SEM cross-section observation using a cryo-microtome. The electrodes were prepared by mixing Si and graphite (1:1 weight ratio) with the binder dissolved in *N*-methyl-2-pyrrolidinone (NMP) in the ratio 10%. The graphite (OMAC1S, 15-μm average particle size) was obtained from Osaka Gas (Japan). The SiO_x powder is the same as that used in Ref. [35]. Since the changes in volume of the Si particles are large upon cycling, the electrochemical properties strongly depend on the binder [35]. The binder used in the Si experiments was algae, chosen because it has been recently proved to give much better electrochemical properties than the conventional poly (vinylidene fluoride) (PVDF) [36]. A small fraction of vapor-grown carbon fibers (2% VGCF from Showa-Denko (Japan)) was added to the electrode composition. These

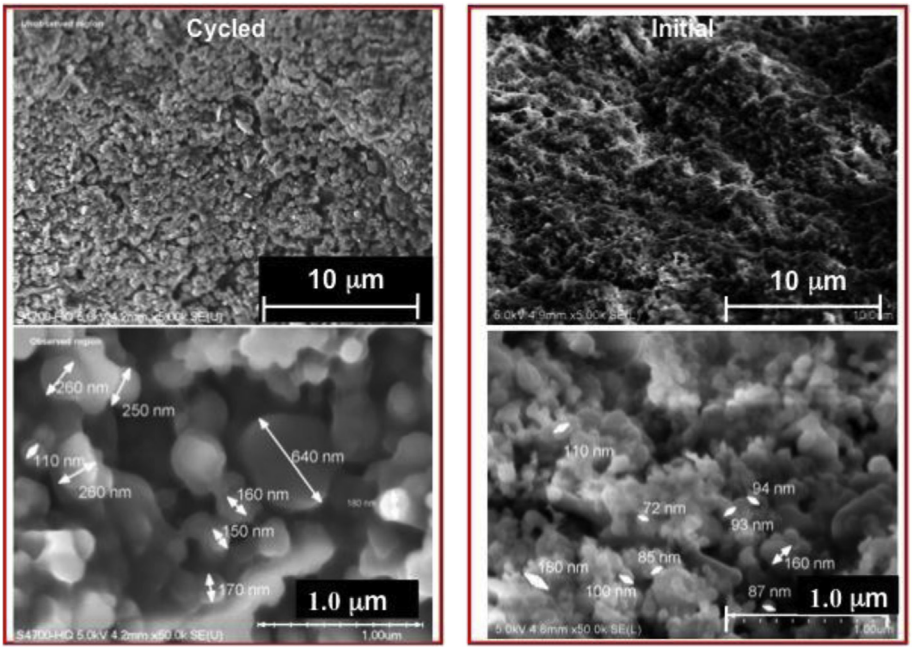

Fig. 1. Right side: Field emission gun (FEG-SEM) images of the Si anode before cycling at two different magnifications. The average size of the Si particles is100 nm. Left side: same electrode after the two cycles shown in Fig. 2.

slurries are coated on copper foil and dried for 24 h at 120 °C under vacuum, and then compressed. The counter electrode was lithium metal. The cells were assembled in an argon-filled glove box. The solid-polymer electrolyte (SPE) chosen for in-situ experiments was a star-shaped polymer having Poly(ethylene oxide) (PEO) arms containing Lithium Bis(Trifluoromethanesulfonyl)Imide (LITFSI) in the ratio of O/Li = 30:1. The cells were pressed one hour to obtain a good Li/SPE interface.

2.2. Electrochemical tests

The ex-situ charge–discharge measurements were carried out on CR2025 coin-type cells with a Li-metal counter electrode, Celgard 3501 separator and electrolyte of 1 M $LiPF_6$ in a mixture of ethylene carbonate (EC) and diethyl carbonate (DEC); in these experiments, discharge refers to the insertion of Li^+ in Si as the cell voltage decreases to 0 V. Charge refers to the extraction of Li from $SiLi_x$ when the voltage increases from 0 to 2.5 V. The tests were evaluated with a multichannel battery cycler (MacPile, Claix, France).

2.3. Characterization

The electrodes using nano-sized Si particles were observed in-situ using a Field emission gun electron microscopy (FEG-SEM) (S-4700, Hitachi, Japan). The electrodes using bigger SiO_x anodes were examined by a Variable pressure SEM (S-3500N, Hitachi, Japan). The same experimental set-up was used recently to investigate the SiO_x–graphite as negative electrode [35]. We have used a FEG-SEM for Si particles because of their smaller size. It was not be possible to see any grain details in the Si experiment using a standard scanning electron microscope (SEM) with a W hairpin source. The FEG used a nano-sized W filament from which the electrons are extracted using a very high electric field. This leads to much higher primary electron brightness (10^8 A cm^{-2} str^{-1} for a FEG against 10^5 for a W hairpin) and, owing to better lenses, a very small spot size even at a lower accelerating voltage and current in order to decrease the deterioration and charging of the materials under investigation. The in-situ SEM observations can be made either plane (top) view or in cross-section view of the electrode. The details on the electrode preparation and the operational procedures of the SEM have been described elsewhere [37–39]. The cells were cycled in a custom build sample holder under a small pressure (<30 psi or equivalently < 206 KPa) at 70 °C.

For ex-situ analysis of SiO_x electrode at different depth of discharge (DOD), the electrodes were observed plan-view, and tranches were prepared in-situ using a 'nano-duet' microscope (NB-5000, Hitachi, Japan).

3. Results on Si electrodes

The SEM image of the nano Si electrode before cycling in Fig. 1 shows that Si particles are poly dispersed with sizes in the range 70–200 nm (average particle size ca. 100 nm). The cycling results for this electrode are illustrated in Fig. 2. We have checked that the capacity 1160 mAh g^{-1} during the first cycle is almost equal to the theoretical one and does not depend on the cycle rate at the low C-rates up to C/15. Then we have reported in Fig. 2 the voltage of the cell that is the only parameter that depends on the C-rate under such conditions up to the end of the cycle. The next cycles are recorded when the current is fixed to the theoretical value corresponding to a charge/discharge at C/15. The difference between the discharge time and the corresponding charge times for the two first cycles gives evidence of the loss of capacity in the second cycle, the shorter time in the charge/discharge being

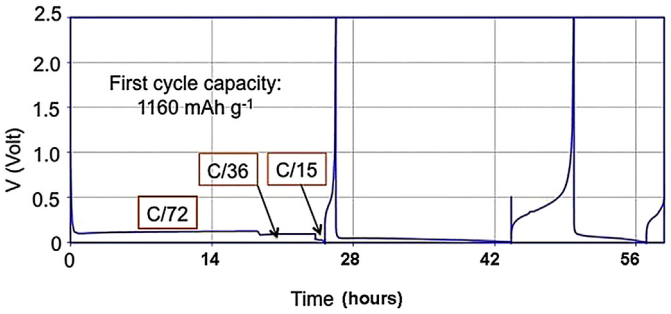

Fig. 2. Cycling performance of the anode made of the Si particles shown in Fig. 1. The C-rate used in the experiments is indicated in the figure.

dictated by the cut-off of the current when the voltage exits from the range 0–2.5 V. The capacity decreases to 1025 mAh g^{-1} in the second cycle. As expected, the in-situ video picturing the evolution of the electrode (Video 1) shows a large change in the volume of the electrode during the cycling. The same observations have been made at different resolutions. The recording at high-resolution in Video 2 illustrates the very large Si expansion observed during the second discharge when the voltage of the cell is in the vicinity of 0.045 V. In this video, the color of the image becomes slightly darker with time, mainly due to carbon deposition/migration of hydro-carbon induced by the electron beam of the SEM (carbon contamination). The same particles behavior is observed at any magnification (lower magnification produce less electron dose and thus lower C deposition). In order to decrease the carbon contamination, no observation was made (i.e. no electron beam was sent to the cell) in the time range [6 h–24 h] in these experiments. The first important result is that no cracking of the particles can be observed. Even the biggest particles (200 nm) did not crack. Another striking result that can be also observed on these videos is the electrochemical sintering of the particles upon cycling. This is best evidenced in Fig. 1 that compares, at two magnifications, Si electrode before and after the two cycles. After the two cycles, those of the particles that did not coalesce (this point will be discussed below) have a volume ca. 85% bigger than before cycling. This dilatation of the particles was not observed after the first cycle; it is observed only after the second one. Nevertheless a significant capacity loss between charge and discharge is observed during this cycle. Wu and Bennett have argued that this loss is due to a consumption of charge associated to the decomposition of the electrolyte to form the solid electrolyte interface (SEI) [40]. On another hand, the amorphization of Si during this first cycle can generate at the second cycle many defects, including dangling bonds that have a strong affinity to capture Li ions [41]. Substituted Li in Si can be kept stable up to 670 °C [42]. Therefore, it may be very difficult to extract all the Li^+ ions from the particle under electrochemical conditions in the second cycle. Taking into account the fact that the volume change $\Delta V/V$ is 420% between Si and $SiLi_{4.4}$, and assuming that the volume change is proportional to the Li content, a 85% volume change after the second cycle would correspond to a Li concentration $SiLi_{0.9}$, and thus a 20% loss of capacity between the first and the second cycle. This is indeed the order of magnitude of the loss of capacity observed in Fig. 2 between the two cycles. Therefore, the main part of the loss of capacity observed in the electrochemical experiments is caused by the decomposition reaction of the electrolyte during the first cycle, but in the second cycle it is mainly attributable to the remaining Li ions that cannot be extracted from the lithium from the structural defects such as dangling bonds generated upon cycling inside the Si particles.

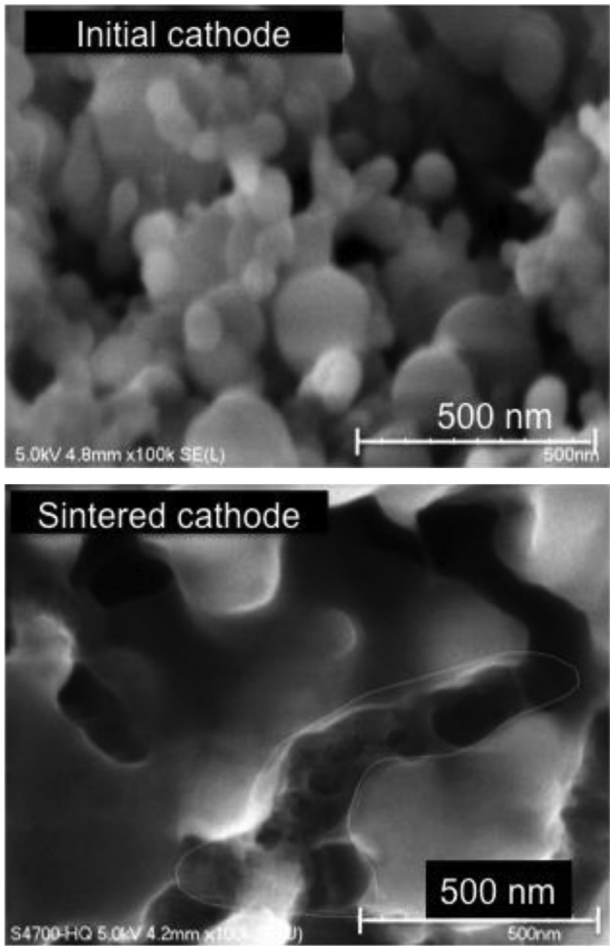

Fig. 3. Electrochemical sintering of the Si particles after the second cycle.

Supplementary video related to this article can be found at http://dx.doi.org/10.1016/j.jpowsour.2013.09.069.

In addition, Si particles aggregate. This is best evidenced in Fig. 3, showing that many dispersed particles have coalesced into a flocculation structure, up to the point where the SEM image detect a continuous net structure with cavities. This phenomenon is the so-called electrochemical sintering [43]. This change in the morphology associated to the aggregation of the particles has been repeatedly observed for nano-sized uncoated Si particles when they are discharged to 0.0 V vs. Li^+/Li [41,44,45]. We find in the present work that this phenomena starts at the second cycle, at potential ca. 0.045 V. The mechanism proposed for this agglomeration mechanism [41] is that the insertion of lithium ions expands the volume of each particle and increases the contact of separated particles. Then, due to the high surface energy of nanosized particles [29], Si atoms of neighbor particles may have a strong affinity to bond together and form an agglomerated body. We find that this process is still active for particles of size of the order of 100 nm.

As a consequence of this electrochemical sintering, the electrode becomes much more rigid, to the point where the electrode cannot accommodate the change of volume upon cycling. The result is a fracture of the electrode already in the next cycle after the sintering has been observed, resulting in the failure of the electrode. This is shown in Video 3 recorded with a cell prepared with nano Si powder and Algae binder.

Supplementary video related to this article can be found at http://dx.doi.org/10.1016/j.jpowsour.2013.09.069.

Several studies have suggested a terminal particle size below which particles do not fracture [46,47]. The fracture of nanosized Si wires, however, contradicts these conclusions [48]. Recently, the recordings of the formation of $Li_{22}Si_5$ nanorods suggest that the Si nanorods with diameters of 26 nm did not fracture upon lithiation, while nanorods with 55 nm were cracked [33,49]. These conflicting results suggest that the cracking of the particles do not only depend only on the size but also on the shape of the particles and on its crystal orientation [33]. More spherical particles are mechanically less fragile than ultrathin nanorods, which might make a difference in the ability of the particles to avoid cracking upon cycling. This could mean the stress in the particle has a preferred direction of propagation. Since the formation of $Li_{22}Si_5$ is damageable to the Si-particles, we might expect that the substitution of Si by SiO particles would avoid the formation of this phase, and thus would prevent the particles from cracking. It is the purpose of the next section to explore the behavior of micron-sized SiO particles of the same shape as in this section.

4. Results on SiO_x anodes

The SiO_x ($x \sim 0.95$) particles used in this work are the same as in our earlier work [35]. SiO is thermodynamically unstable. The commercial SiO is then constituted of nanoclusters of amorphous Si clusters and amorphous SiO_2 clusters, surrounded by Si-suboxide [50,51]. The suboxide part is expected to be inactive in the chemical process. Advantage has been taken this property by using SiO as a buffer to constrain the volume change of the active part [52]. Therefore, the mechanical properties of Si and SiO are not necessarily the same. Even the electrochemical properties of SiO cannot be extrapolated from Si. The electrochemical reactions of SiO involved during cycling are still controversial, with formation of new phases in different concentrations (Li_2O, Li–Si alloy and Li–silicates) [53–58].

We have performed the same experiments as in the former section on micron-sized SiO particles to investigate the cracking upon cycling. Fig. 4 gives the SEM image of the working electrode, showing the size distribution ranging from 6 to 20 μm. The electrochemical properties are reported in Fig. 5 under the form of the voltage as a function of time at constant current 0.05 mA, corresponding to a charge–discharge at rate C/12. In these experiments, the cycles are restricted to the voltage range 0.1–2.5 V. Under such conditions, the capacity is 1120 mAh g^{-1} and remains constant along the three first cycles that have been explored, which gives evidence that the particles did not crack. This is confirmed by the SEM images recorded in-situ (Video 4), and in Fig. 4 at the end of the discharge at 0.1 V in the two first cycles (same time scale as in Fig. 5). During the Li insertion, the image in Fig. 4 gives evidence of a reversible increase/decrease of the size of the particles upon insertion/extraction of Li. No cracking can be observed when the voltage is kept larger than 0.1 V. The difference in the backscattered electron (BSE) intensity of the particles in Fig. 4 before cycling and after discharge is due to the fact that the BSE intensity is a function of the mean atomic number of the target and thus, on the Li-content, as it is shown in Fig. 6, and computed using the Casino Monte-Carlo program [59]. Therefore, the non-lithiated part of the particles is whiter (more BSE intensity) in the image. On another hand, upon Li insertion, the BSE intensity is lower and the particle becomes darker and darker.

Supplementary video related to this article can be found at http://dx.doi.org/10.1016/j.jpowsour.2013.09.069.

We can see clearly in the Video 4 and Fig. 4 that even at the end of the discharge (picture at $V = 0.11$ V), part of the bigger particles remain white, i.e. the lithium did not have sufficient time to diffuse inside their core region. This result explains the rather low capacity

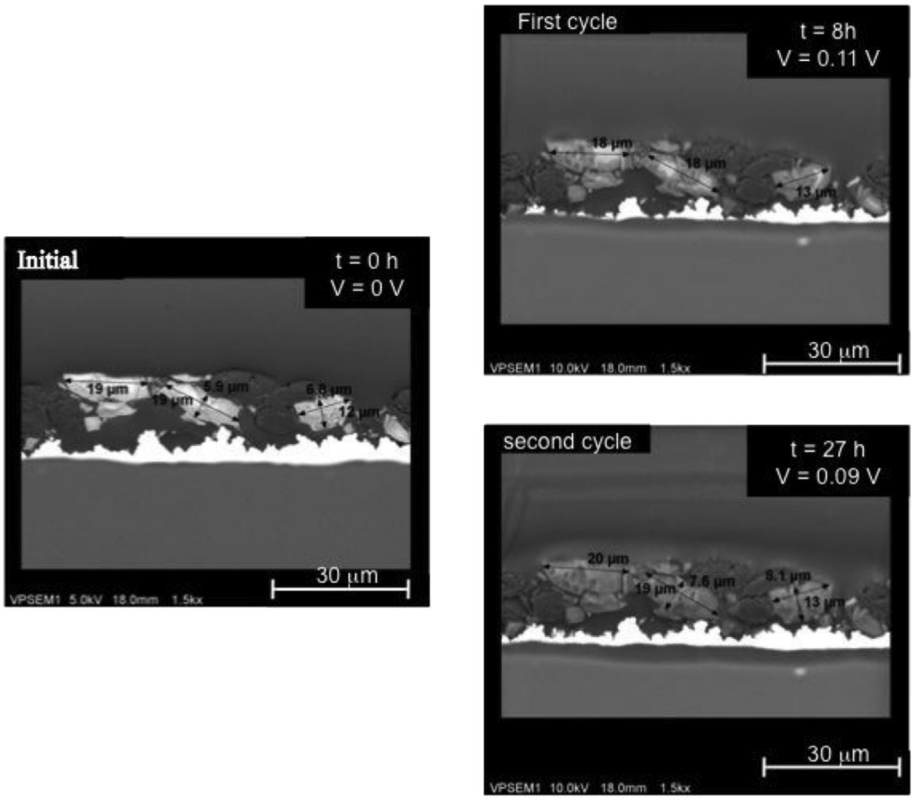

Fig. 4. Cross-section image of the electrode made with micron-sized SiO particles before cycling (to the left), and at the end of the discharge limited to $V = 0.1$ V in the first and second cycles, along the cycling tests reported in Fig. 5.

observed with such particles. In addition, it gives evidence that the system is out of thermodynamic equilibrium. We can see in Fig. 7 that the opposite holds true, i.e. at the end of charge at 2.5 V, part of the particles are not white, confirming the difficulty to extract all the lithium.

Some gas evaporation was clearly visible during in-situ experiment (see Fig. 7), which was responsible for the very short filament life (<30 h instead of 100 h in absence of gas evaporation). This evaporation is presumably due to the reductive decomposition of LiTFSI. We have chosen this salt for the ability of the TFSI anion to form passivating surface films during electro-reduction in the presence of Li ions, and LiTFSI is also known for its highest conductivity in dry polymer. However, the study of the decomposition of ionic liquid during cathodic polarization of lithium and graphite electrodes has revealed that the decomposition of this anion results in the production of volatile products, mainly trifluoromethane [60].

Small trenched regions at the electrode surface were obtained in-situ using a focused ion beam on the SiO electrode (Fig. 8). We also present result of X-ray mapping using an energy dispersive X-ray spectroscopy (EDS) of the same part of the electrode. The SiO particles are poly-disperse in the range 1–10 µm, and embedded

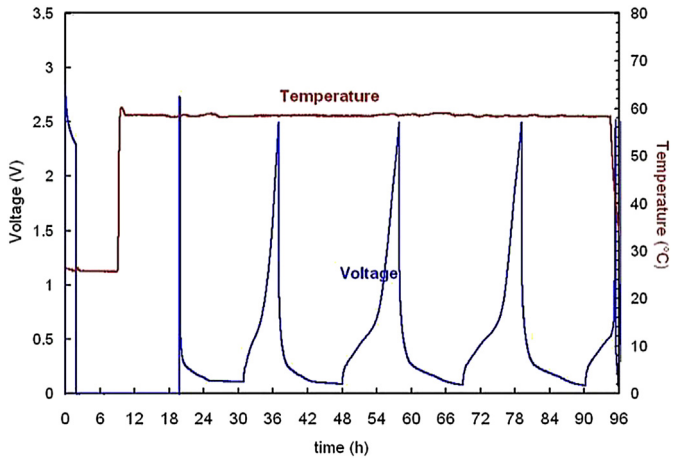

Fig. 5. Cycling of the electrode with micron-sized SiO particles in the voltage range 0.1–2.5 V. The time scale is the same as the one used in Fig. 4.

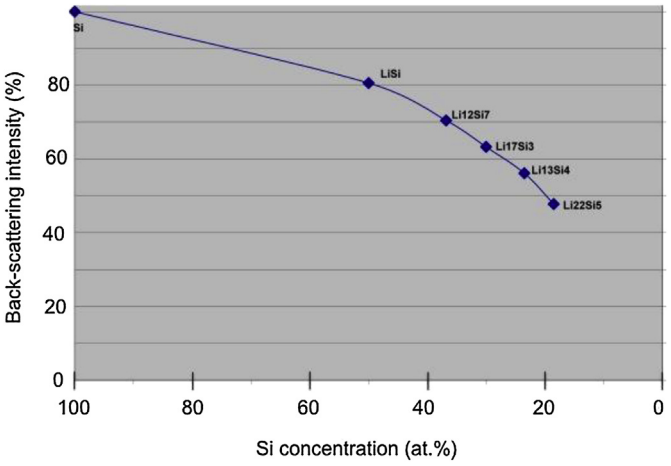

Fig. 6. Intensity of the backscattered electron as a function of the Li concentration x in $SiLi_x$ normalized to Si and computed using the Casino Monte-Carlo program [59].

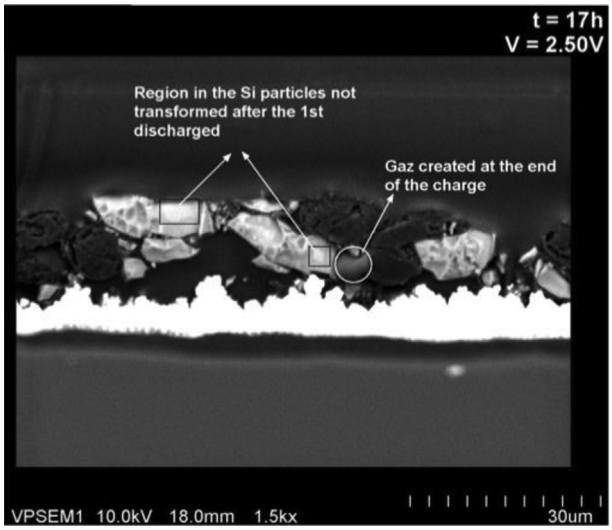

Fig. 7. Cross-section image of the electrode made with micron-sized SiO particles at the end of charge (2.5 V).

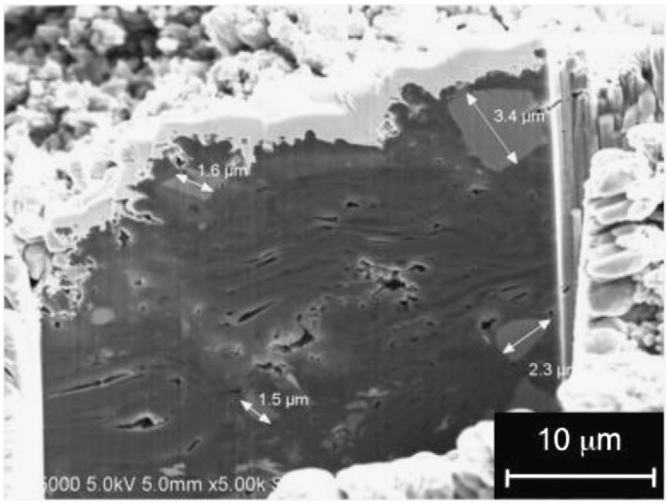

Fig. 9. Cross-section image of the electrode made with micron-sized SiO particles after deep discharge at 15 mV. Note the crack near the surface of the 3.4 µm particle at the upper right corner of the image.

in the organic medium made of the electrolyte and binder. In addition, the image shows that this medium is very porous, aiming to absorb the large change of volume of the SiO particles. Fig. 9 shows the same electrode after the first full discharge ($V = 5$ mV) at rate C/24. The very large volume increase of the particles has now compacted the electrode. In addition, the X-ray mapping images in Fig. 10 shows an important change in the structure of the electrode, since the oxygen has now spread outside the particles, suggesting the production of Li_2O, while Si particles are formed.

This formation of Si allows us to understand now why the particles did not crack when the voltage is maintained larger or equal to 0.1 V. This threshold corresponds to the voltage expected for the composition $Li_{12}Si_7$. Indeed, Bridel et al. [61] have reported that the Si-particles do not fracture when they are not solicited entirely (stop of the lithiation at $Li_{12}Si_7$ instead of $Li_{22}Si_5$). On another hand, they crack when the lithiation process is pushed up to the formation of $Li_{22}Si_5$. Therefore, one advantage of the formation of Si upon cycling of SiO particles is the reduced fatigue of the electrode when the voltage is kept above 0.1 V.

The drawback of the loss of oxygen, however, is that the substitution of Si by SiO particles in the pristine electrode cannot lead to any improvement of its mechanical resistance when the cycling involves deep discharge at 15 mV. This is confirmed by the observation of Fig. 9. On one hand, the smaller particles of size $d < 2$ µm have conserved their integrity. On another hand, the bigger particles have cracked. This can be observed for the particle with $d = 3.4$ µm on top right of Fig. 9, or in Fig. 10 as well. In these two figures, the particles have cracked near the surface. But, the big particles $d > 10$ µm have been pulverized. This is illustrated in Fig. 11. Therefore, we find that the change of volume of the SiO particles is comparable to that of the Si particles, contrary to a hypothesis in Ref. [35]. Instead, our result confirms that the limited volume change of the SiO/C electrodes does not come from the

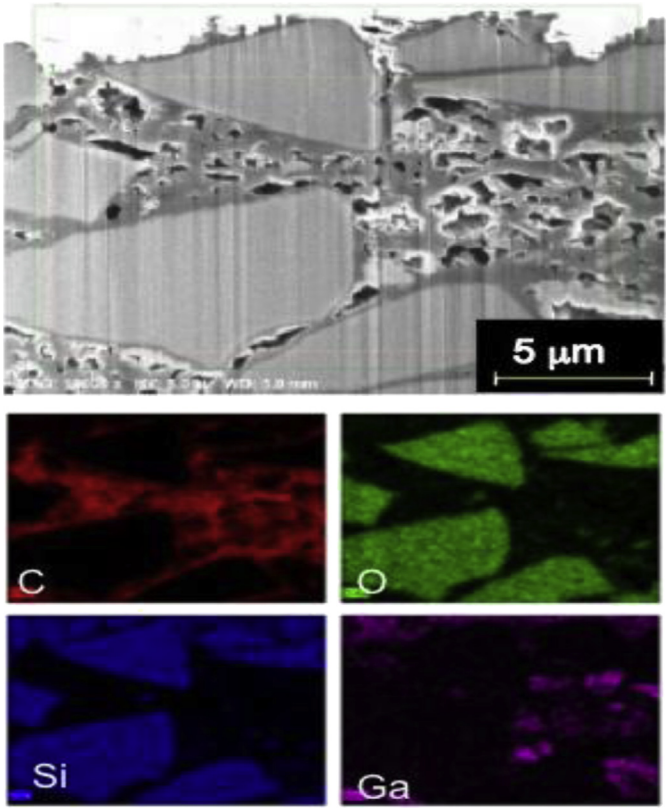

Fig. 8. Cross-section image of the electrode made with micron-sized SiO particles before cycling (top), and EDS analysis (down) showing the Si and O elements inside he particles, and carbon from the binder and the electrolyte.

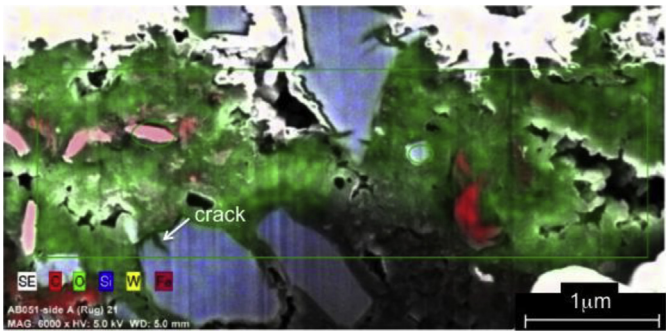

Fig. 10. X-ray mapping of the SiO cell after deep discharge at $V = 15$ mV. Note the important O increase in the binder/electrolyte compared to Fig. 8.

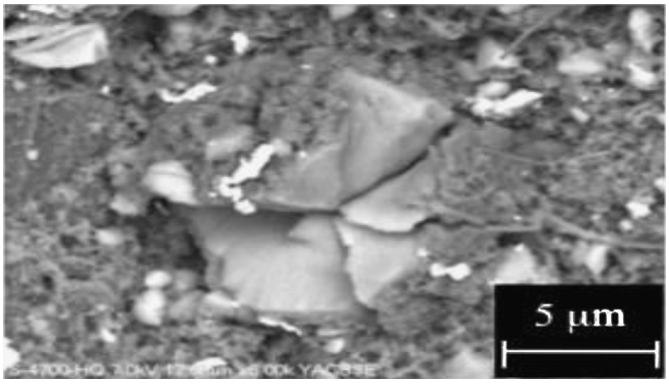

Fig. 11. Example of pulverized SiO particle after the deep discharge.

particles, but the increase of pre-formed voids between the particles in presence of carbon, so that the these voids can be filled and emptied during cycling [62].

5. Conclusion

The in-situ electron microscopy of Si and SiO-based electrodes with different sizes of particles between 0.1 and 20 μm has provided a new insight into the micro-structural evolution of the particles. When the particles are larger than 10 μm, the cell is out of thermodynamic equilibrium even at low C/24 rate, because the lithium ions do not have time enough to exit from the particles. The consequence is an inhomogeneous distribution of Li in the particles that can increase the internal stress during cycling. Nevertheless, rather big (micron-sized) SiO particles resist and conserve their integrity when the voltage of the battery is limited to 0.1 V, i.e. when the lithiation is stopped at $Li_{12}Si_7$. The substitution of Si by SiO does not help, as the oxygen is lost during the cycling. On another end, full discharge results in a cracking of the particles of dimension $d > 2$ μm near the surface, and the particles with $d > 10$ μm are pulverized. On another hand, with the smaller particles ($d \sim 0.1$ μm), the electrochemical sintering is a cause of failure of the battery, because the more rigid electrode cracks. These results suggest that Si cannot be competitive with lithium or even graphite, unless the clamped hollow nanostructures that avoid these problems can be synthesized at a price that is not prohibitive for a commercial use.

Acknowledgments

BATT-DOE (US) and HydroQuébec and are gratefully acknowledged for the financial support.

References

[1] K. Zaghib, A. Guerfi, P. Hovington, A. Vijh, M. Trudeau, A. Mauger, J.B. Goodenough, C.M. Julien, J. Power Sources 232 (2013) 357.
[2] K. Zaghib, A. Mauger, H. Groult, J.B. Goodenough, C.M. Julien, Materials 6 (2013) 1.
[3] K. Zaghib, A. Mauger, J. Goodenough, C.M. Julien, in: D. Lockwood (Ed.), Nanotechnology for Li-ion Batteries, Springer Verlag, Berlin, 2011 (Chapter 8).
[4] M.V. Reddy, G.V. Subba Rao, B.V.R. Chowdari, Chem. Rev. 113 (7) (2013) 5364–5457.
[5] K. Zaghib, M. Dontigny, A. Guerfy, P. Charest, I. Rodrigues, A. Mauger, C. Julien, J. Power Sources 196 (2011) 3949.
[6] K. Zaghib, M. Dontigny, A. Guerfi, J. Trottier, J. Hamel-Paquet, V. Gariepy, K. Galoutov, P. Hovington, A. Mauger, H. Groult, C.M. Julien, J. Power Sources 216 (2012) 192–200.
[7] M.N. Obrovac, L. Christenzen, D.B. Le, J.R. Dahn, J. Electrochem. Soc. 154 (2007) A849.
[8] K. Kobayashi, S. Seki, Y. Ohno, H. Miyashiro, P. Charest, A. Guerfi, K. Zaghib, J. Power Sources 185 (2008) 542.
[9] H.S. Kim, K.Y. Chung, B.W. Cho, J. Power Sources 189 (2009) 108.
[10] T. Takamura, S. Ohara, M. Uehara, J. Suzuki, K. Sekine, J. Power Sources 129 (2004) 96.
[11] X. Yang, Z. Wen, X. Xu, B. Lin, Z. Lin, J. Electrochem. Soc. 153 (2006) A1351.
[12] D. Larcher, S. Beattie, M. Mocrette, K. Edstrom, J.-C. Jumas, J.M. Tarascon, J. Mater. Chem. 17 (2007) 3759.
[13] K. Zaghib, J. Dubé, A. Dallaire, K. Galoustov, A. Guerfi, M. Ramanathan, A. Benmayza, J. Prakash, A. Mauger, C.M. Julien, Handbook on Lithium-ion Battery Applications, Elsevier, 2013.
[14] J.R. Szczech, S. Jin, Energy Environ. Sci. 4 (2011) 56.
[15] J.O. Besenhard, J. Yang, M. Winter, J. Power Sources 68 (1997) 87.
[16] L.Y. Beaulieu, K.W. Eberman, R.L. Turner, L.J. Krause, J.R. Dahn, Electrochem. Solid-State Lett. 4 (2001) A137.
[17] L.Y. Beaulieu, T.D. Hatchard, A. Bonakdarpour, M.D. Fleischauer, J.R. Dahn, J. Electrochem. Soc. 150 (2003) A1457.
[18] X.W. Zhang, P.K. Patil, C.S. Wang, A.J. Appleby, F.E. Little, D.L. Cocke, J. Power Sources 125 (2004) 206–213.
[19] C.K. Chan, H.L. Peng, G. Liu, K. McIlwrath, X.F. Zhang, R.A. Huggins, Y. Cui, Nat. Nanotechnol. 3 (2008) 31.
[20] M.T. McDowell, S.W. Lee, C. Wang, Y. Cui, Nano Energy 1 (2012) 401.
[21] U. Maver, A. Znidarsic, M. Gaberscek, J. Mater. Chem. 21 (2011) 4071.
[22] S.K. Soni, B.W. Sheldon, X.C. Xiao, M.W. Verbrugge, D. Ahn, H. Haftbaradaran, H.J. Gao, J. Electrochem. Soc. 159 (2012) A38.
[23] K.L. Lee, J.Y. Jung, S.W. Lee, H.S. Moon, J.W. Park, J. Power Sources 129 (2004) 270.
[24] M.S. Park, G.X. Wang, H.K. Liu, S.X. Dou, Electrochim. Acta 51 (2006) 5246.
[25] P.R. Raimann, N.S. Hochgatterer, C. Korepp, K.C. Moller, M. Winter, H. Schrottner, F. Hofer, J.O. Besenhard, Ionics 12 (2006) 253.
[26] C.M. Park, J.H. Kim, H. Kim, H.J. Sohn, Chem. Soc. Rev. 39 (2010) 3115.
[27] G.K. Simon, T. Goswami, Metall. Mater. Trans. A Phys. Metall. Mater. Sci. 42A (2011) 231.
[28] W.J. Zhang, J. Power Sources 196 (2011) 13.
[29] H. Wu, Y. Cui, Nano Today 7 (2012) 414.
[30] H. Wu, G. Chan, J.W. Choi, Y. Ryu, Y. Yao, M.T. McDowell, S.W. Lee, A. Jackson, Y. Yang, L.B. Hu, Y. Cui, Nature nanotechnology 7 (2012) 309.
[31] J.Y. Huang, L. Zhong, C.M. Wang, J.P. Sullivan, W. Xu, L.Q. Zhang, S.X. Mao, N.S. Hudak, X.H. Liu, A. Subramanian, H.Y. Fan, L.A. Qi, A. Kushima, J. Li, Science 330 (2010) 1515.
[32] Y.M. Sun, X.L. Hu, W.X. Zhang, L.X. Yuan, Y.H. Huang, J. Nanopart. Res. 13 (2011) 3139.
[33] X.H. Liu, H. Zheng, L. Zhong, S. Huan, K. Karki, L.Q. Zhang, Y. Liu, A. Kushima, W.T. Liang, J.W. Wang, J.H. Cho, E. Epstein, S.A. Dayeh, S.T. Picraux, T. Zhu, J. Li, J.P. Sullivan, J. Cum-ings, C.S. Wang, S.X. Mao, Z.Z. Ye, S.L. Zhang, J.Y. Huang, Nano Lett. 11 (2011) 3312.
[34] X.H. Liu, L.Q. Zhang, L. Zhong, Y. Liu, H. Zheng, J.W. Wang, J.H. Cho, S.A. Dayeh, S.T. Picraux, J.P. Sullivan, S.X. Mao, Z.Z. Ye, J.Y. Huang, Nano Lett. 11 (2011) 2251.
[35] A. Guerfi, P. Charest, M. Dontigny, J. Trottier, M. Lagacé, P. Hovington, A. Vijh, K. Zaghib, J. Power Sources 196 (2011) 5667.
[36] I. Kovalenko, B. Zdyrko, A. Magasinski, B. Hertzberg, Z. Milicev, R. Burtovyy, I. Luzinov, G. Yushin, Science 334 (2011) 75.
[37] K. Zaghib, P. Hovington, M. Lagacé, A. Guerfi, P. Charest, K. Zaghib, C.M. Julien, J. Prakash (Eds.), ECS Proceeding Volume PV 2003–20, New Trends in Intercalation Compounds for Energy Storage and Conversion, The Electrochemical Society, Pennington, NJ, 2003, p. 670.
[38] K. Zaghib, M. Armand, M. Gauthier, J. Electrochem. Soc. 145 (1998) 3135.
[39] K. Zaghib, M. Armand, M. Gauthier, J. Broadhead, B. Scrosati (Eds.), Proceedings of the Symposium on Lithium Polymer Batteries, The Electrochemical Society, Pennington, NJ, 1997, p. 250.
[40] J. Wu, R. Bennett, 2012 IEEE Energy Tech Conference, Cleveland, OH, United States, 29–31 May 2012.
[41] H. Li, X. Huang, L. Chen, G. Zhou, Z. Zhang, D. Yu, Y.J. Mo, N. Pei, Solid State Ionics 135 (2000) 181.
[42] W. Wahl, H. Hofsaaa, S.G. Hahn, S. Winter, E. Recknagei, Appl. Phys. Lett. 62 (1993) 684.
[43] J.T. Vaughey, K.D. Keplar, D.R. Vissers, M.M. Thackeray, in: Abstracts of the 9th International Meeting on Lithium Batteries, Edinburgh, Scotland, July, 1998.
[44] H. Li, X.J. Huang, L.Q. Chen, J.Q. Li, Y.Q. Zhou, Z.G. Wu, Y. Liang, Solid State Ionics 135 (2000) 181.
[45] H. Li, X.J. Huang, L.Q. Chen, Electrochem. Solid-State Lett. 1 (1998) 241.
[46] R.A. Huggins, W.D. Nix, Ionics 6 (2000) 57.
[47] J. Yang, M. Winter, J.O. Besenhard, Solid State Ionics 90 (1996) 281.
[48] U. Kasavajjula, C. Wang, A. Appleby, J. Power Sources 163 (2007) 1003.
[49] H. Ghassemi, M. Au, N. Chen, P.A. Heiden, R.S. Yassar, ACS Nano 5 (2011) 7805.
[50] A. Hohl, T. Wieder, P.A. Aken, T.E. Weirich, G. Denninger, M. Vidal, S. Oswald, C. Deneke, J. Mayer, H. Fuess, J. Non-Cryst. Solids 320 (2003) 255.
[51] K. Schulmeister, W. Mader, J. Non-Cryst. Solids 320 (2003) 143.
[52] Yoon Hwa, Cheol-Min Park, Hun-Joon Sohn, J. Power Sources 222 (2013) 129.
[53] M. Miyachi, H. Yamamoto, H. Kawai, T. Ohta, M.J. Shirakata, J. Electrochem. Soc. 152 (2005) A2089.
[54] J. Yang, Y. Takeda, N. Imanishi, C. Capiglia, J.Y. Xie, O. Yamamoto, Solid State Ionics 152–153 (2002) 125.
[55] M. Miyachi, H. Yamamoto, H. Kawai, J. Electrochem. Soc. 154 (2007) A376.
[56] T. Kim, S. Park, S.M. Oh, J. Electrochem. Soc. 154 (2007) A1112.
[57] Y. Nagao, H. Sakaguchi, H. Honda, T. Fukunaga, T. Esaka, J. Electrochem. Soc. 151 (2004) A1572.

[58] J.-H. Kim, C.-M. Park, H. Kim, Y.-J. Kim, H.-J. Sohn, Electroanal. Chem. 1 (2011) 664.
[59] P. Hovington, D. Drouin, R. Gauvin, Scanning 19 (1997) 1–14.
[60] E. Markevich, R. Sharabi, V. Borgel, H. Gottlieb, G. Salitra, D. Aurbach, G. Semrau, M.A. Schmidt, Electrochim. Acta 55 (2010) 2687.
[61] J.-S. Bridel, T. Azaïs, M. Morcrette, J.-M. Tarascon, D. Larcher, J. Electrochem. Soc. 158 (2011) A750.
[62] W.-R. Liu, Y.-C. Yen, H.-C. Wu, M. Winter, N.-L. Wu, J. Appl. Electrochem. 39 (2009) 1643.